

Automatic detection on the bolt loose based on digital image processing

* Yu Liu¹⁾, Lin-sheng HUO²⁾ and Gang-bing Song³⁾

^{1), 2)} *State Key Laboratory of Coastal and Offshore Engineering, Dalian University of Technology, Dalian, Liaoning 116024, China*

³⁾ *Smart Materials and Structures Laboratory, Department of Mechanical Engineering, University of Houston, Houston, TX 77204, USA*

¹⁾ liuyu35@mail.dlut.edu.cn

ABSTRACT

Bolt connection is an important form of steel bridge connection. The looseness of the connection node often leads to fatigue damage, which is one of the main reasons of the steel member damage in the bridge. In general, loose bolts are visually inspected by inspectors to assess health status. However, visual inspections are time-consuming, expensive, dangerous and easy to make error. With the development and maturity of image processing technology and aerial photography technology, image processing can be applied to loose bolt detection of large-scale bridge structures, which is an automatic and rapid detected method to ensure the safety during detection process. In this study, we identified the rotation angle of the nut from the images obtained by the drone, by the following steps: First, the aerial drone collected the bolt photos. and then, the images were corrected by image processing techniques and bolt edges were extracted. Finally, determining the angle of each bolt and calculating the rotation angle. An algorithm for detecting the loosening angle of bolts was produced through this idea. We verified the applicability of this method through a set of simulation experiments. The results demonstrated that the measurement error of this method was less than 5.5%, which suggested that this method could accurately detect the looseness of bolts. The main innovation of this method is the combination of drone and digital image processing (DIP), which makes the whole detection process fast, accurate and safe.

KEYWORDS: *Unmanned Aerial Vehicle, Digital Image Processing, Bolt loose, Steel bridges*

¹⁾ Ph.D. Candidate

²⁾ Associate Professor

³⁾ Professor

1. Introduction

In long-span steel bridges (Wu, Chen and Lindt, 2012), high-rise buildings and large transmission towers, bolts are important elements to connect members of structures. (Fisher, Mertz and Zhong, 1983)



Figure 1 Examples of loosened bolts
picture from:

(https://media2.architecturemedia.net/site_media/media/cache/24/48/2448954dec6d33603c3861646e713e43.jpg)

Fatigue damage to the connecting nodes is one of the major forms of damage to the steel members of the bridge. (Alessio Pipinato, Marco Molinari, Carlo Pellegrino, Bursi and Claudio Modena, 2011) Therefore, the design of steel connections and node structure become very important. In the connection of steel structure, high-strength bolt is the most common method of connection. However, many reasons may lead to the loosening of high-strength bolts at the connection nodes so that the structural effectiveness would be reduced or even destroyed, especially the bridge structure under dynamic load. From the status of steel bridges using high strength bolts all over the world, the failure of joints often begins with the looseness of high strength bolts. (Harik, Zhao and Hu, 2011) (Albrecht, Sahli and Wattar, 1987, Yang, 1998, Hou, Xiong, Tian and Wang, 2001)

A variety of techniques have been developed to detect bolt-loosening. (Wang, Song, Liu, Li and Xiao, 2013, Qiao and Esmaeily, 2011, Qiao, Esmaeily and Melhem, 2008) The loss of bolt's preload could be identified by using nondestructive techniques such as: the guided wave method, impedance method, the magnet field method, the vibration measurements method and the electric potential drop method. The guided wave-based technique utilizes the change in the ultrasonic wave generated by the piezoelectric transducer, which is passing through the splice plate, to detect the bolt-loosening. (Park, Yun and Roh, 2006, Kim and Hong, 2009) The received ultrasonic wave is altered when the loss of bolt preload changes the dynamic characteristics of the splice plate. The impedance-based method has high sensitivity to the local structural damage and the wide frequency bandwidth. It is specially fitted for monitoring bolted joints, which are dominated by local dynamics of high-frequency characteristics. (Sohn, Farrar and Inman, 2003, Kim, Park, Hong and Ho, 2011, Huynh, Lee and Kim, 2015) The magnet field-based method is based on a simple phenomenon in which the bolt-loosening is caused by rotating a nut and this rotation changes magnetic field around the nut. (Gotoh, Komori and Ueno, 2016) The vibration measurements method developed a new damage index based on the difference of frequency response functions on the slab and the corresponding points on the girder to evaluate the condition of shear connectors. (Xia, Hao, Deeks and Zhu, 2008) The electric potential drop method uses the relationship between the electrical resistance and the change in thickness of a steel splice plate to

alarm the bolt-loosening. If a bolt is loosened, the cross-section area of the splice plate is increased, making the electric resistance decreased.(Shimamura, Mukai, Todoroki and Kobayashi, 2001)

Despite their potentials for bolt-loosening monitoring, the above-mentioned methods need high-cost data acquisition systems and also require a number of sensors to cover all bolts in a large-sized connection. In addition, changes in conditions such as temperature variation could affect the accuracy of bolt-loosening detection since structural responses as well as sensing materials used in these techniques are temperature-dependent.(BAO, XIA, LI, XU and ZHANG, 2012) Hence, an alternative monitoring technique should be sought for in-situ health monitoring or inspection of large-scale bolted connections in structures..(Esmaily, 2013)

In engineering practice, the current troubleshooting for the bolt has the following major problems:

(1). Most troubleshooting of bolts still rely on manual inspection, and its reliability depends on the expert's working status and proficiency.(Results, Results, Remarks, Brent, Rolander, Graybeal and Glenn, 2001)

(2). The complicated structure of the parts and the messy background further enhance the difficulty of detecting the key bolt.

Up-to-date, with the rapid development of computer science, the research of recognition technology based on image information has become mature and practical. Image processing techniques have been widely adopted to recognize medical images, objects, patterns, characters and so on.(Nuruzzaman) Many researchers have made their attempts to utilize the techniques for inspection and monitoring of civil structures.(VikramPakrashi, FranckSchoefs, JeanBernardMemet and AlanO'Connor, 2010) For example, the techniques were used to identify cracks on concrete(Abdelqader, Abudayyeh and Kelly, 2003, Hutchinson and Chen, 2006, Yamaguchi and Hashimoto, 2010, Liu, Cho, Spencer and Fan, 2016, Ghorbani, Matta and Sutton, 2014) and pavement surface(Subirats, Dumoulin, Legeay and Barba, 2007, Zou, Cao, Li, Mao and Wang, 2012, Li, Sun, Tan and Ning, 2012), to detect and evaluate corrosion occurred in steel structures(Choi and Kim, 2005, Lee, Chang and Skibniewski, 2006), to detect damage on the surface of stay cables in cable-stayed bridges(Ho, Kim, Park and Lee, 2013), and to measure displacement of the bridge(Fukuda, Feng, Narita, Kaneko and Tanaka, 2013). The main advantages of image-based bridge structure technology are as follows: First, it provides intuitive, quantitative, and temperature-independent information for structural maintenance. Second, the cost is low. Finally, it is possible to use only one camera to inspect large areas on buildings.

For bolt lose testing based on image technology, many scholars have done a lot of research in this field. Cha et al(Cha, You and Choi, 2016) proposed the bolt loose detection method based on Huff transformation and support vector machine. However, these methods still exist the problem such as expensive, non-automatic and low accuracy. Thus, an algorithm using image processing techniques to identify bolt looseness in steel structures has been proposed. we identified the rotation angle of the nut from the images obtained by the drone, by the following steps: First, taking a picture for a bolt joint. Then, segmenting the images for each nut by image processing techniques and finally identifying rotation angle of each nut and detecting bolt-loosening. Threshold cutting technology and canny edge detection algorithm are used as the key

technology of image processing, affine transformation algorithm is used as the theoretical basis for image correction. By using the powerful image processing software Halcon, an automatic measurement of bolt angle has been achieved. A drone has been used to simulate real-world experiments to verify the applicability of our method. The experimental results demonstrate that the method can be used for bolt looseness detection in practical engineering.

2. method

2.1 Image point arithmetic

Image point arithmetic, being a pixel-by-pixel operation, refers to the performance of the same gray transform on each pixel in the image, which only changes the gray value of the pixel except for the spatial relationship between the pixels. Assuming that p and q denote the grayscale values of the input image $P(x,y)$ and the output image $Q(x,y)$ at the point (x,y) respectively, the image point operation may be expressed by equation (1):

$$q = T(p) \quad (1)$$

Where T represents the operator of the point, which is kind of gray-scale mapping relation between input image and output image. In general, Image point arithmetic is utilized to change the image gray value range and distribution, and sometimes to be an important tool of image digitization.

2.2 Noise and noise reduction methods

When the camera captures images, a certain range of random changes will occur in the collected image gray values due to various environmental factors. This change in the gray value of the captured image is called as noise, which is ubiquitous and cannot be eliminated completely in the image acquisition process. The noise mainly concentrates on the high frequency region of Fourier transform in the image. The common noise is Gaussian noise, Rayleigh noise and impulse noise. (Vu, Tran, Nguyen and Hariharan, 2014, Steger, Ulrich and Wiedemann, 2007) For the image noise suppression, Gaussian filtering, mean filtering, median filtering and other image smoothing method are often used to complete. (Gupta, 2007) In this paper, Gaussian filter method has been used for image noise reduction.

The pixel gray value $v_{r,c}$, which is not affected by noise, has its column number r , and its line number c . The noise is a stationary random process under normal circumstances, which is expressed by $n_{r,c}$. Then the pixel gray value under the noise interference is $\overline{v_{r,c}} = v_{r,c} + n_{r,c}$. Gaussian filter uses the form of convolution to calculate the new gray value of the pixel. The correlation of each pixel in a Gaussian filter is related to the distance to the center pixel. Its equation is as equation (2):

$$f_{\sigma}(r,c) = \frac{1}{2\pi\sigma^2} e^{-\frac{(r^2+c^2)}{2\sigma^2}} \quad (2)$$

Where r represents the longitudinal distance between other pixels and the central pixel, and c represents the lateral distance between other pixels and the central pixel. It can be seen from (2) that the closer to the central pixel, the higher the correlation is. In

addition, the farther the pixel farther from the center pixel is, the lower the correlation is. When the distance from the center pixel exceeds 4-unit pixel lengths, the correlation basically approaches zero. It means that it appropriately increases the weight of the center of the filter, and the weight decreases rapidly away from the center, which ensures that the gray value of the center point is closer to the pixel point that is closer to it. The advantage of this principle is to make the gray value of the calculation distribute more reasonably. In sum, compared with other filtering methods, Gaussian filter algorithm, which can better preserve the contour of target object and suppress high frequency noise at the same time, is almost the best algorithm in current image smoothing method.

2.3 Grayscale threshold segmentation

Each pixel of digital image has 266 gray levels which range from 0 to 255 gray value. A grayscale image with a grayscale threshold of 0-255 displays a black-gray-white image effect as a whole. In fact, Grayscale changes gradually. 0 represents pure black and 255 represents pure white. Gray threshold transformation can be defined in this way: assuming a fixed value is between 0 and 255. If the grayscale image pixel grayscale value is less than the grayscale value, the grayscale value of the pixel is set to 0; if the grayscale image pixel gray is greater than the gray value, the gray value of the pixel is set to 255. After the gray-scale threshold transforms, the gray-scale image will become a black-and-white binary image, and the image has only two kinds of grayscale values: 0 and 255, meaning the image is either black or white. The gray value of this definition acts as a dividing line and is therefore called the threshold. Using the function expression to describe the gray threshold transform is shown as equation (3) :

$$f(x) = \begin{cases} 0 & x < T \\ 255 & x \geq T \end{cases} \quad (3)$$

Where T is the user-set threshold. Grayscale threshold transform is widely used, it is also one of the important methods of image segmentation. By converting a grayscale image into a binary image and setting a suitable threshold, it can be directly extracted the interest-area from the complex background.

2.4 Feature Extraction and Morphology Processing

2.4.1 Regional characteristics

The main purpose of the image processing is to find the area of bolt. In order to find the area of interest, we should start from the features of the areas themselves, separating the area from other areas according to these features, and finally extracting them separately from the images. The most common and easiest feature is area, which is expressed as $S = |R|$, Where $|R|$ denotes the number of pixels contained in the region, and since the area of one pixel in the image is unit 1, $|R|$ indicates the area of the region. There are two areas in Figure 2. The area of the left hexagon is 1468 and the area of the right hexagon is 1413. Then we use the area threshold of 1400-1450 and there will be only the right hexagonal left.

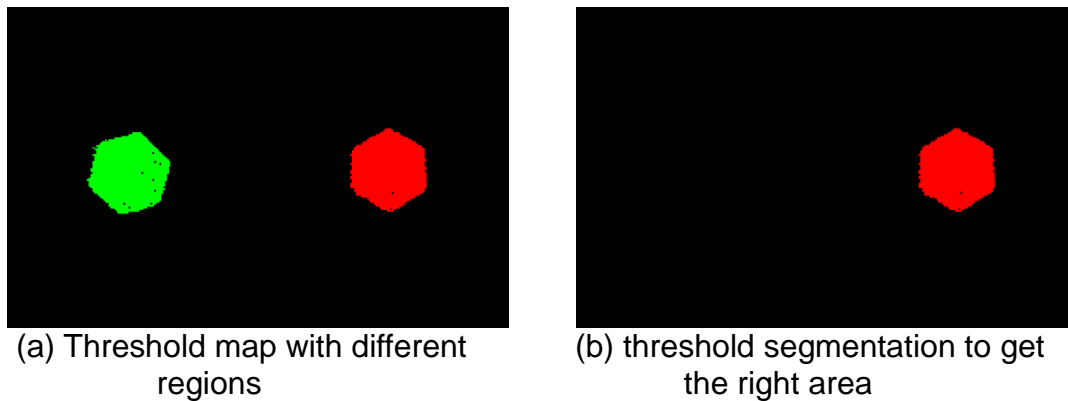


Figure 2 Threshold segmentation results

2.4.2 Minkowski addition and expansion

The first type operator in morphological processing is Minkowski addition, which is showed in Equation (4) :

$$R + R_s = R \cup R_s \quad (4)$$

Where R represents the area to be processed, and S represents the law of processing R . S is a structuring element, which is usually represented by a vector. R shift through the S vector will finally get the area R_s . R_s and R themselves take the union of the region which is obtained after the Minkowski addition result area. The principle is shown in Figure 3, where the vector of S is one unit to the right and down.

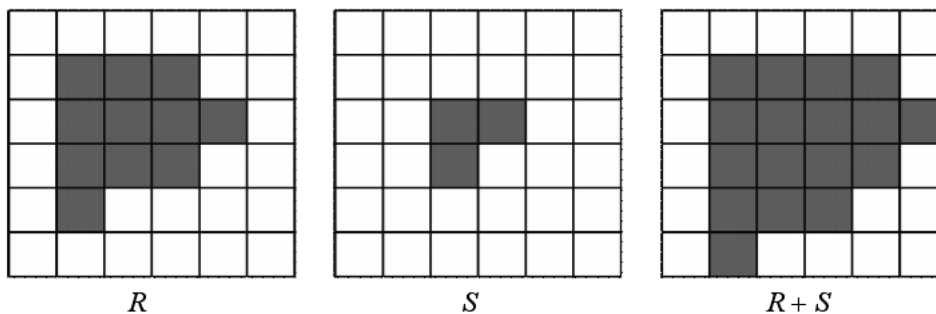


Figure 3 Examples of Minkowski addition

If the translation vector S in Minkowski's addition is transposed symmetrically with respect to itself, the transposed vector is \bar{S} . Replace \bar{S} in Equation (4) with the translation vector S , this operation is called expansion. We do the expansion of S with respect to R in Figure 3 and the result is shown in Figure 4. Expansion operations in HALCON are equivalent to Minkowski addition. Expansion and Minkowski addition both enlarge the area of processing, therefore, the unsplit multiple regions in the image can be converted into separate regions which use the extension method.

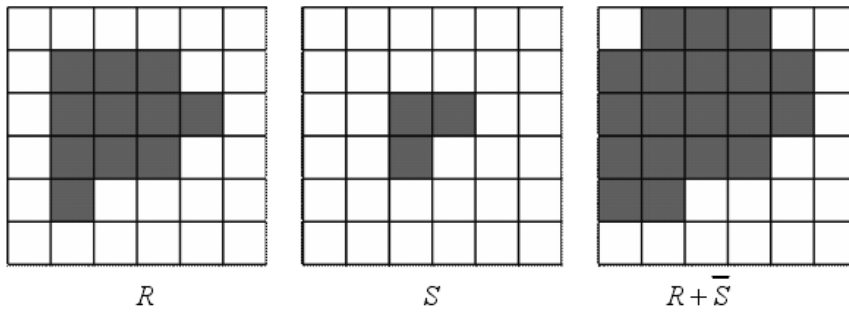


Figure 4 Examples of expansion

2.4.3 Minkowski subtraction and corrosion

Minkowski subtraction is the second type operator in morphological processing. By changing the union symbol in Minkowski's summation to the intersection symbol, we get the definition of Minkowski subtraction, which is shown in equation (5) :

$$R + R_s = R \cap R_s \quad (5)$$

In equation (5), R shift through the S vector will finally get the area R_s . R_s and R themselves take the intersection of the region is obtained after the Minkowski subtraction result area. The principle is shown in Figure 5, where the vector of S is one unit to the right and down.

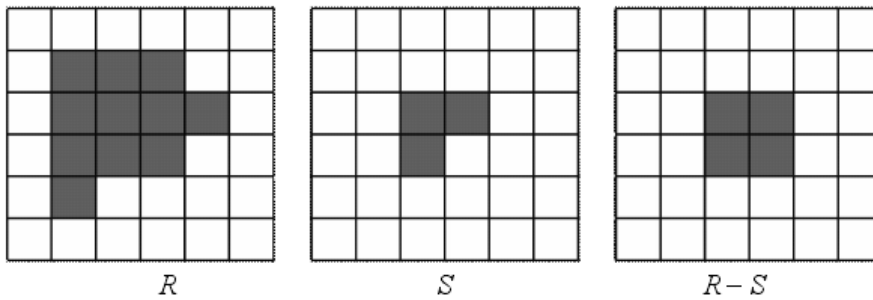


Figure 5 Examples of Minkowski subtraction

If the translation vector S in Minkowski's subtraction is transposed symmetrically with respect to itself, the transposed vector is \bar{S} . Replace \bar{S} in Equation (5) with the translation vector S, this operation is called corrosion. The corrosion of S with respect to R is shown in Figure 6. Corrosion treatment will make the object area smaller, it can play the role of separation of objects connected to each other.

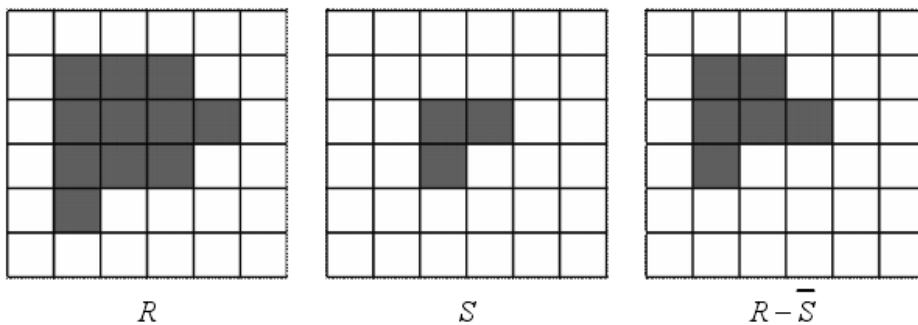


Figure 6 Examples of corrosion

2.4.4 Canny edge detector

Canny Edge Detector(Canny, 1986) is a commonly used gradient-based edge detection methods. Like other methods, Canny detector is a convolution filter while it's a bit more complex and powerful. This method uses a Gaussian mask as the best smooth filter to eliminate the noise in the image while other gradient-based methods (especially the Sobel and Prewitt methods) use an averaging filter(Abdelqader, Abudayyeh and Kelly, 2003). We get the definition of Gaussian G in two-dimensional space, as shown in the following equation:

$$G = e^{-\frac{x^2+y^2}{2\sigma^2}} \quad (6)$$

Where σ is the standard deviation.

After the image is smoothed by a Gaussian filter, the Canny detector calculates the gradient modulus of each pixel in the X and Y directions and the direction of the gradient. The central differential masks D_x and D_y in the X and Y directions are defined as:

$$D_x = [-1 \ 0 \ 1] \quad D_y = [-1 \ 0 \ 1]^T \quad (7)$$

The gradient D and direction θ_g in a pixel can be calculated as:

$$D = \sqrt{(I_{sub} \cdot Dx)^2 + (I_{sub} \cdot Dy)^2}, \quad \theta_g = \tan^{-1}\left(\frac{I_{sub} \cdot Dy}{I_{sub} \cdot Dx}\right) \quad (8)$$

Where I_{sub} is an arbitrary sub-image with 3×3 pixels in the image. and (\cdot) denotes a convolution operator. Convolution is the process of multiplying entries and sums that are similar in position.

After calculating the gradient of all pixels in the image by non-maximum suppression, which is to find local maximum for the gradients. Next, the potential edge is detected again with two thresholds (a so-called high threshold th_H and a low threshold th_L). Noting that the other edge detectors use only one threshold, which makes two thresholds-using an unique feature of Canny detectors. If the gradient values of the pixels are greater than the high threshold, they are marked as strong edge pixels. If all pixels are greater than the low threshold gradient value except the strong edge pixels, they are labeled as weak edge pixels.

Finally, the real edge is detected by hysteresis tracking the potential edges. Strong edge pixels should be participated in the final edge image. If any weak edge pixels are connected to a strong edge pixel, we select it as the true edge. Otherwise, it is removed.

2.4.5 Contour segmentation

Supposing a contour is composed of n points, if its first point and then point are the same. this Contour is a closed contour. As you can see in Figure 7, virtually every side of the bolt outline is connected end to end by many small segments, which are not hexagons in the standard sense. Thus we cannot measure the angle of each side. To solve this problem, a hexagon could be used to fit the outer contour. This hexagon fit is achieved by the Rammer algorithm, which is the best of all polygon fit algorithms.(Ramer, 1972) Figure 8 illustrates how the Rammer algorithm works. For a non-closed contour, firstly connecting one of its two ends with a line, then looking for the point on the contour that is farthest from the line. If the distance from this point to the line segment is greater

than a threshold set previously, then the current contour line is divided into two segments at this contour point. Next, the above processing is repeated on the two newly-separated contour lines, and the operation is repeated until all the segments satisfy the contour point while the maximum distance between the two segments is less than or equal to the set threshold. The closed contours are firstly divided into two non-closed contours by an arbitrary segment, and then the cycle operation is started again until the requirement is met. For the closed contour, the number of contour points which meet the conditions is the same as the number of segments separated from the closed contours.

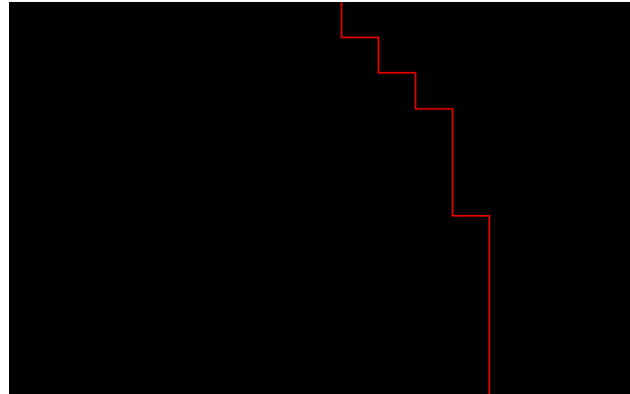


Figure 7 Detail of bolt edge

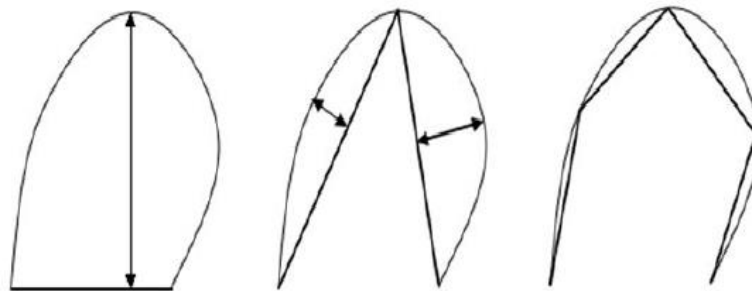
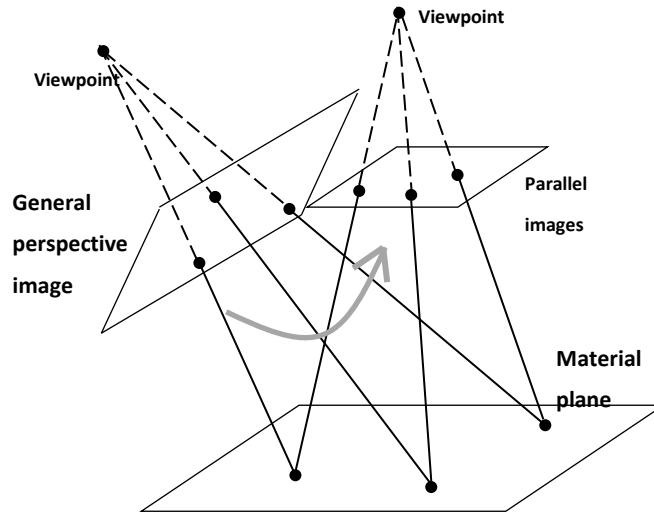


Figure 8 Rammer algorithm uses recursive subdivision example, the thin line is the outline, the thick line represents the approximation polygon

2.4.6 Affine transformation

For angle measurement between straight lines, if the captured image is a positive image, you can measure the angle directly from the image. In actual shooting, it is difficult to ensure the parallel relationship between the photographic plane and the positive projection plane of the object. Normally the captured image is a general perspective image, as shown in Figure 9, which does not have the measurement characteristics. Therefore, before measuring, it requires to be changed to a parallel image (parallel to the object orthographic projection plane) by the correction approach.

Figure 9 Diagram of projection transformation



In fluoroscopic imaging, there is a projective transformation between the general perspective image and the parallel image. In the projective plane, points and lines in a general fluoroscopic image are represented by homogeneous coordinates, described as follows $p = (x_1, x_2, x_3)^T$, $l = (l_1, l_2, l_3)^T$, $p^S = (x_1^S, x_2^S, x_3^S)^T$, $l^S = (l_1^S, l_2^S, l_3^S)^T$ respectively represent points and straight line parallel to the image, the projective transformation relationship is shown as equation (9) and equation (10):

$$p^S = H * p \quad (9) \quad l^S = H^{-T} * l \quad (10)$$

Where H is a third-order homography matrix, which can be decomposed into the following form, shown as equation(11):

$$H = H_p H_A H_s = \begin{pmatrix} I & 0 \\ v^T & 1 \end{pmatrix} \begin{pmatrix} K & 0 \\ 0^T & 1 \end{pmatrix} \begin{pmatrix} sR & t \\ 0^T & 1 \end{pmatrix} \quad (11)$$

Where H_p is a projective transformation matrix, H_A is an affine transformation matrix, and H_s is a similar transformation matrix. K in H_A is a combination of transition and non-uniform scaling. (Olver and Tannenbaum, 2003)

This decomposition is true without considering the special case where the infinity line in the parallel image becomes the origin of the coordinates in the perspective image. The uniqueness of the decomposition is related to the sign of s, and s is got from normalizing the upper triangular matrix without affecting the uniqueness of the projective transformation matrix H_p and the affine transformation matrix H_A .

The projective transformation H_p , can be corrected to a general perspective image parallel images, but cannot correct the image measurement features. Meanwhile, the affine transformation H_A only corrects the measurement characteristics without changing the relationship between the image and the orthographic projection plane of the object. The similarity transformation H_s only performs the transformation such as rotation, translation, zooming and reflection on the image and does not affect the measurement characteristics of the image and the image The relationship between the positive projection plane of the object. Therefore, in angle detection, similar

transformations are not considered, that is, there is no need to consider the influence of normalization on the uniqueness of decomposition.

According to the above analysis, firstly, we must projective transformation of the image. The transformation matrix can be constructed by a straight line corresponding to two parallel sets of parallel lines that are not parallel to each other in parallel images, To solve the vanishing point of two parallel lines, two vanishing points can determine a straight line $l = (l_1, l_2, l_3)^T$, This line should correspond to an infinite line in the parallel image plane. As shown in Figure 10 (general perspective image). When $l_3 = 0$, the straight line passes through the coordinate origin, which belongs to a special case not being considered in this paper. Therefore, we assume $l_3 \neq 0$. At this point, we construct the projective transformation matrix as:

$$H_P^{-1} = \begin{pmatrix} 1 & 0 & 0 \\ 0 & 1 & 0 \\ l_1 & l_2 & l_3 \end{pmatrix} \quad (12)$$

It's easy to verify, $(0,0,1)^T = H_P^{-1}l$, In this way, the line of an infinite straight line in the image plane is restored to infinity, that is, the parallel relationship between straight lines is corrected. However, the angle between the lines is not completely restored, as shown in Figure 10(affine image), which requires to be corrected by affine transformation. In projective geometry, the cosine of the angle θ of any two straight lines $l = (l_1, l_2, l_3)^T$ and $m = (m_1, m_2, m_3)^T$ is calculated as equation(13)::

$$\cos \theta = \frac{l^T C_\infty^* m}{\sqrt{(l^T C_\infty^* l)(m^T C_\infty^* m)}} \quad (13)$$

Among them, to meet $C_\infty^* = H_S C_\infty^* H_S^T$, C_∞^* is a quadratic curve, called the dual point of the circle point.

Supposing $l^S = (l_1^S, l_2^S, l_3^S)^T$ and $m^S = (m_1^S, m_2^S, m_3^S)^T$ are two lines which is perpendicular to each other in a parallel image, then we can get equation (14):

$$l^{ST} C_\infty^* m^S = 0 \quad (14)$$

Assuming that $l^P = (l_1^P, l_2^P, l_3^P)^T$ and $m^P = (m_1^P, m_2^P, m_3^P)^T$ are respectively the corresponding straight lines of the straight lines l and m in the affine image plane, then according to equation (9) (10)and (11), we can get equation (15):

$$l^{PT} (H_A C_\infty^* H_A^T) m^{PT} = l^{PT} \begin{pmatrix} KK^T & 0 \\ 0 & 0 \end{pmatrix} m^{PT} = 0 \quad (15)$$

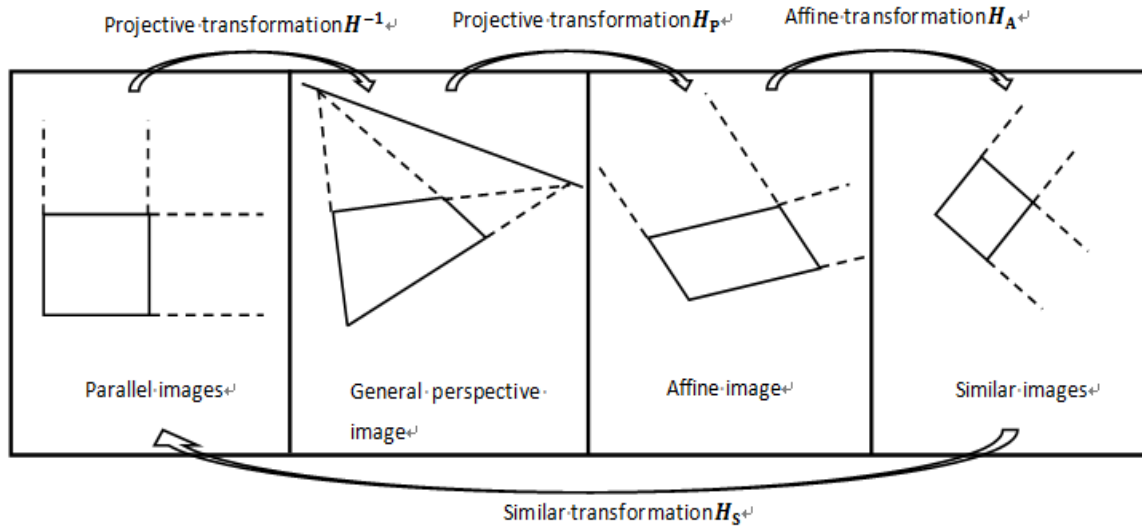


Figure 10 Diagram of line rectify

In this way, K can be obtained from two groups of vertical lines that are not parallel to each other in the parallel image, and then we can get the affine transformation matrix H_A .

After two-step correction process with projective transformation H_P , affine transformation H_A , the two straight lines in the image plane $l = (l_1, l_2, l_3)^T$ and $m = (m_1, m_2, m_3)^T$ has been resumed as the same angle relationship with the corresponding straight line in the parallel image.

$$\begin{pmatrix} l_1^A & l_2^A & l_3^A \\ m_1^A & m_2^A & m_3^A \end{pmatrix} = \begin{pmatrix} l_1 & l_2 & l_3 \\ m_1 & m_2 & m_3 \end{pmatrix} H_P H_A \quad (16)$$

Where $l^A = (l_1^A, l_2^A, l_3^A)^T$ and $m^A = (m_1^A, m_2^A, m_3^A)^T$ are respectively the corresponding straight lines of the straight lines l and m in the similar image plane.

Based on the above principle, with HALCON's powerful image processing capabilities, a method has been proposed which could automatically correct the image according to the aspect ratio of any rectangle on any two-dimensional image. Firstly, the rectangular bottom plate is extracted by the image processing method. Then, using the known ratio of the length of the rectangular floor, the conversion matrix can be found directly to achieve image correction.

3. Experimental verification

Bolting is an important part of the bridge structure like long-span steel bridge. In this study, a bolting group experiment which simulated the actual bridge condition was established to verify the applicability of this method to detect bolt looseness. As shown in Figure 11, the bolt cluster connection model consists of a rectangular steel plate, bolts

and nuts. The rectangular plate is 26cm long, 15cm wide and 14mm thick. Three sets of standard bolts and nuts M24 are mounted on the base plate. The floor is silvery white, the bolt is painted with red anti-rust paint.



Figure 11 Test model

The photographs of the model were taken using a professional UAV Advanced Aerial Vehicle (DJI Inspire1 RAW) with a focal length of $f = 20$ mm, a 1 / 2.3-inch CMOS sensor and a photo pixel of 12.4 million. The pictures were taken by the autofocus function when the distance between the camera and the model was 50-100 cm

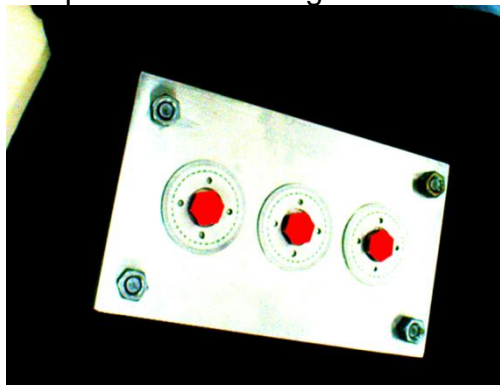


Figure 12 UAV

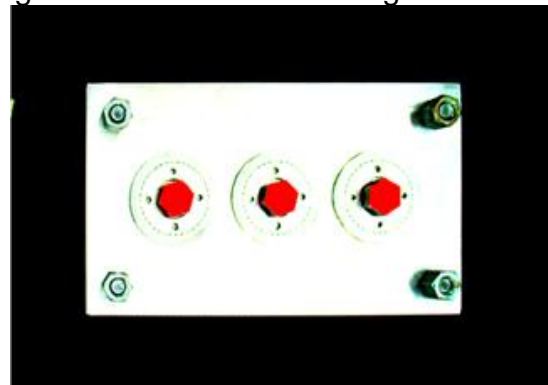


Figure 13 Bolt groups shot at different angles before loosening by UAV

In order to detect the loosening occurrence in the bolted joint model and evaluate the feasibility of this method, we set a series of experiments with different degrees of bolt looseness. We used a drone to take a picture of bolt groups from different angles, which have not been loosened. As shown in Figure 13. Then use affine transformation algorithm to correct the image, which is shown in Figure 14. After that we used image processing method to analyze the collected pictures. First, we use Gaussian filter method to filter the picture and which is shown in Figure 15. Then we used the threshold segmentation technique to extract the bolt under test, and then repair the extracted region by Minkowski algorithm. After that, we used the Canny edge operator to extract the bolt edge, and segment the edge using Ramer algorithm, which can be seen in Figure 16, 17 and 18. Finally we draw the perspective of each side, shown in Table 1. The bolts and the numbers of each side in Table 1 are shown in Figure 19. In Table 1, it displays the angles of the bolts obtained after the bolt groups are taken from different angles. The radian represented the angle between the edge and the horizontal straight line.

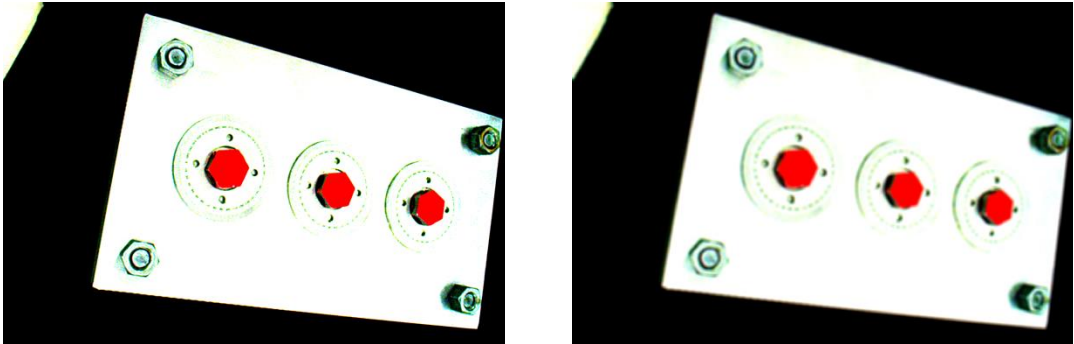


(a) Bolt group images are taken at any angle



(b) Affine Transform Correction of Bolt Group Image

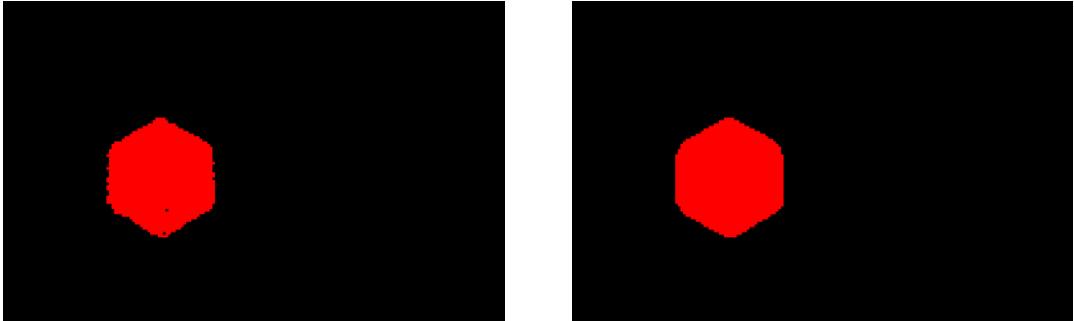
Figure 14 Affine transformation correction



(a) Normal photo

(b) Gaussian filtered photo

Figure 15 Gaussian filter processing



(a) Before morphological transformation

(b) After morphological transformation

Figure 16 Morphological transformation

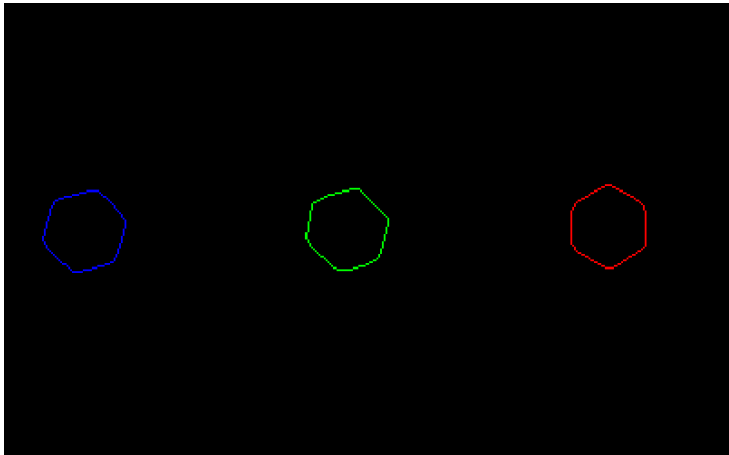


Figure 17 Bolt edge line after edge extraction by Canny edge detector

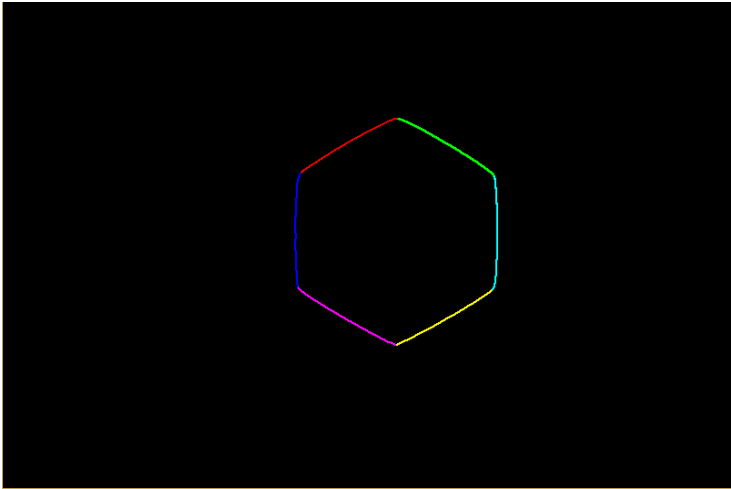


Figure 18 Use the RAMMER algorithm to segment the bolt edge line

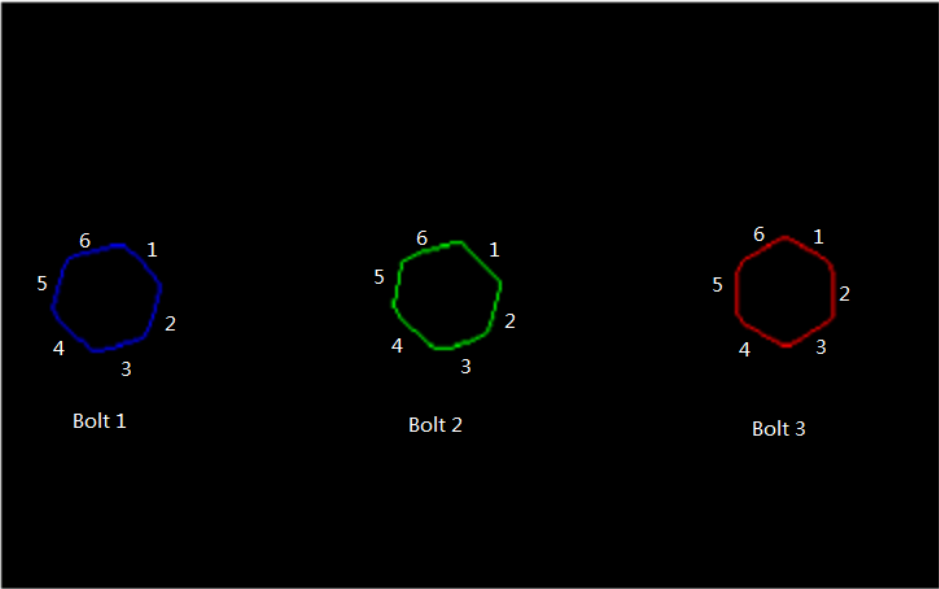


Figure 19 The number of bolt group

Bolt	Side	Angle	Bolt	Side	Angle
Bolt 1	1	2.48365	Bolt 1	1	2.48365
	2	1.45224		2	1.45224
	3	-2.71924		3	-2.71924
	4	-0.763117		4	-0.763117
	5	-1.74044		5	-1.74044
	6	0.373434		6	0.373434
Bolt 2	1	2.58998	Bolt 2	1	2.58998
	2	-1.58844		2	-1.58844
	3	-2.68446		3	-2.68446
	4	-0.571739		4	-0.571739
	5	1.60905		5	1.60905
	6	0.474264		6	0.474264
Bolt 3	1	2.17069	Bolt 3	1	2.17069
	2	1.16415		2	1.16415
	3	0.0762518		3	0.0762518
	4	2.05498		4	2.05498
	5	1.04586		5	1.04586
	6	0.140287		6	0.140287

Table 1 angles of the bolts obtained after the bolt groups are taken at different angles

Then we used NDI Optotrack three-dimensional measurement system to verify the accuracy of this method. The NDI Optotrack 3D Measurement System is a measurement device that tracks the location of active marker points based on optical principles in a given space. We turned the bolt after the device connected, and then the acquisition device recorded the appropriate angle of rotation. After the recording completed, the drone collected the image of the bolt group with the same rotation angle. We compared the parameters obtained by the three-dimensional measurement system with the bolt angles obtained by the image processing, and the corresponding results are shown in Table 2.

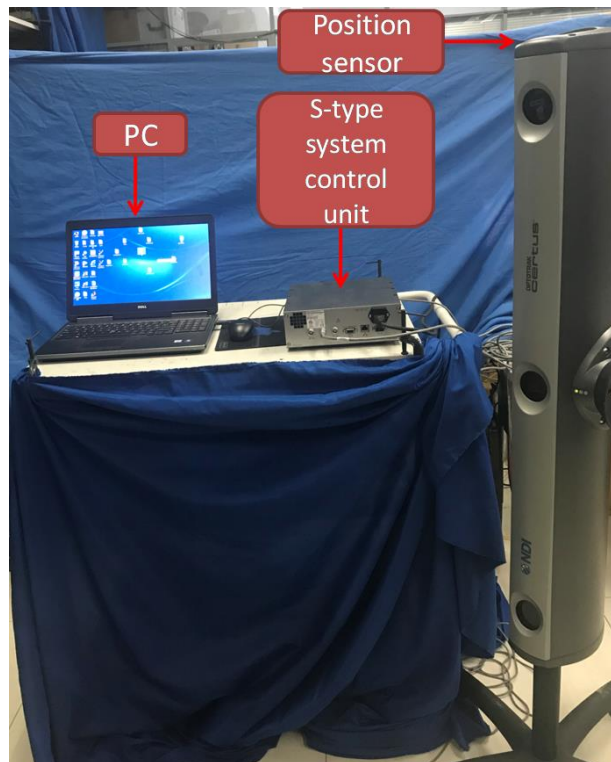


Figure 20 NDI Optotrak three-dimensional measurement system

Rotate a certain angle	Side 1 $\Delta\theta$	Side 2 $\Delta\theta$	Side 3 $\Delta\theta$	Side 4 $\Delta\theta$	Side 5 $\Delta\theta$	Side 6 $\Delta\theta$	average	Standard deviation	Measured value	Relative error
Bolt 1	8.425	8.411	8.817	8.663	8.447	8.828	8.599	0.179	8.885	0.032
Bolt 2	11.995	12.243	12.291	12.361	12.504	12.345	12.290	0.154	12.642	0.028
Bolt 3	10.038	10.202	10.078	10.660	10.341	10.280	10.267	0.205	10.6172	0.033

Rotate a certain angle	Side 1 $\Delta\theta$	Side 2 $\Delta\theta$	Side 3 $\Delta\theta$	Side 4 $\Delta\theta$	Side 5 $\Delta\theta$	Side 6 $\Delta\theta$	average	Standard deviation	Measured value	Relative error
Bolt 1	23.970	23.018	23.233	23.340	22.932	23.436	23.322	0.338	22.133	0.032
Bolt 2	17.975	17.263	17.182	17.691	17.285	17.276	17.445	0.288	18.158	0.028
Bolt 3	15.812	15.874	15.981	15.849	16.463	16.079	16.010	0.221	16.829	0.033

Rotation angle	Side 1 $\Delta\theta$	Side 2 $\Delta\theta$	Side 3 $\Delta\theta$	Side 4 $\Delta\theta$	Side 5 $\Delta\theta$	Side 6 $\Delta\theta$	average	Standard deviation	Measured value	Relative error
Bolt 1	26.607	26.506	27.156	26.178	26.571	26.359	26.563	0.302	25.348	0.048
Bolt 2	23.907	23.660	23.218	24.050	23.970	23.745	23.758	0.275	22.959	0.035
Bolt 3	31.399	31.044	30.933	31.387	31.222	30.999	31.164	0.184	29.940	0.041

Table 2 According to the proposed method of experimental evaluation of the loose situation

As shown in table 2, three bolts were loosened by a certain angle respectively and the actual value of the bolt rotation angle was measured by means of an NDI Optotrack three-dimensional measuring system. the change of nut angle ($\Delta\theta$) referred to the change in the angle of rotation of the nut as measured by the goniometer before and after loosening. In order to evaluate the accuracy of the method, each loose scene were taken 5-8 photos. photo resolution was 2250*4000 pixels, focal length 20mm. UAV position was not fixed during taking pictures. The images were analyzed by the loosening scene are processed by image processing to calculate the angle of each edge. Then, the angle of loosening of each edge was obtained by comparing the corresponding edge angle with the initial image before loosening. The result showed that the loosening angles detected by each side are the same with the standard deviation less than 0.35. The result of the test is compared with the rotation angle measured by the NDI Optotrack three-dimensional measuring system. Measured value indicated the bolt rotation measured by the NDI system. The result demonstrated that the loosening angle obtained from the photograph was consistent with the rotation angle measured by the three-dimensional measuring system. By evaluating the results of multiple images, the maximum and minimum error of image processing techniques were only 1.81 degrees and 0.0426 degrees respectively. The relative error between the mean value and the measured value is within 6%.

4. Conclusion

This paper presents an algorithm based on image processing to detect bolt looseness. We identified the rotation angle of the nut from the images obtained by the drone, by the following steps: First, the aerial drone collected the bolt photos. and then, the images were corrected by image processing techniques and bolt edges were extracted. Finally, determining the angle of each bolt and calculating the rotation angle.

An algorithm for detecting the loosening angle of bolts was produced through this idea. We verified the applicability of this method through a set of simulation experiments. From the experimental the results can be concluded as follows: (1) The relative error of this technology is within 5.5%, which could meet the requirements of practical engineering. (2) The UAV could reach all parts of the large bridge structure and capture images, which proves the applicability of this method to the real structure.

5. References

- Wu, J., Chen, S., and Lindt, J. W. V. D. (2012). "Fatigue Assessment of Slender Long-Span Bridges: Reliability Approach." *Journal of Bridge Engineering*, 17(1), 47-57.
- Fisher, J. W., Mertz, D. R., and Zhong, A. (1983). "Steel bridge members under variable amplitude, long life fatigue loading, Final report, September 1983,85p." *Nchrp Report*.
- AlessioPipinato, MarcoMolinari, CarloPellegrino, Bursi, O., and ClaudioModena (2011). "Fatigue tests on riveted steel elements taken from a railway bridge." *Structure & Infrastructure Engineering*, 7(12), 907-920.
- Harik, I., Zhao, T., and Hu, J. (2011). *Testing and seismic evaluation of long span steel truss bridges*.
- Albrecht, P., Sahli, A. H., and Wattar, F. (1987). "Fatigue Strength of Bolted Joints." *Journal of Structural Engineering*, 113(8), 1834-1849.
- Yang, J. (1998). "Relaxation in high-strength bolted connections with galvanized steel." *Journal of Bridge Engineering*, 5(2), 99-106.
- Hou, L. I., Xiong, J., Tian, Y. U., and Wang, T. (2001). "The Technique of Integral Node of Steel Truss Girder." *Journal of Hubei Polytechnic University*.
- Wang, T., Song, G., Liu, S., Li, Y., and Xiao, H. (2013). "Review of Bolted Connection Monitoring." *International Journal of Distributed Sensor Networks*,2013,(2013-12-12), 2013(2), 1-8.
- Qiao, L., and Esmaeily, A. (2011). "An Overview of Signal-Based Damage Detection Methods." *Applied Mechanics & Materials*, 94-96, 834-851.
- Qiao, L., Esmaeily, A., and Melhem, H. G. (2008). "Structural Damage Detection Using Signal Pattern-Recognition." *Key Engineering Materials*, 400-402, 465-470.
- Park, S., Yun, C. B., and Roh, Y. (2006). "Active Sensing-based Real-time Nondestructive Evaluations for Steel Bridge Members." *Ksce Journal of Civil Engineering*, 10, 33-39.
- Kim, N., and Hong, M. (2009). "Measurement of axial stress using mode-converted ultrasound." *Ndt & E International*, 42(3), 164-169.
- Sohn, H., Farrar, C. R., and Inman, D. J. (2003). "Overview of Piezoelectric Impedance-Based Health Monitoring and Path Forward." *Shock & Vibration Digest*, 35(6), 451-463.
- Kim, J. T., Park, J. H., Hong, D. S., and Ho, D. D. (2011). "Hybrid acceleration-impedance sensor nodes on Imote2-platform for damage monitoring in steel girder connections." *Smart Structures & Systems*, 7(7), 393-416.
- Huynh, T. C., Lee, K. S., and Kim, J. T. (2015). "Local dynamic characteristics of PZT impedance interface on tendon anchorage under prestress force variation." *Smart Structures & Systems*, 15(2), 375-393.

- Gotoh, Y., Komori, H., and Ueno, J. (2016). "Proposal of slack inspection method of high tension bolt of hexagon head using alternating magnetic field." 1-8.
- Xia, Y., Hao, H., Deeks, A. J., and Zhu, X. (2008). "Condition Assessment of Shear mConnectors in Slab-Girder Bridges via Vibration Measurements." *Journal of Bridge Engineering*, 13(1), 43-54.
- Shimamura, Y., Mukai, S., Todoroki, A., and Kobayashi, H. (2001). "Damage Detection of Bolted Joint in Composite Laminates Using Electric Potential Method." *日本複合材料学会研究発表講演会予稿集*, 2001, 353-354.
- BAO, Y., XIA, Y., LI, H., XU, Y.-L., and ZHANG, P. (2012). "DATA FUSION-BASED STRUCTURAL DAMAGE DETECTION UNDER VARYING TEMPERATURE CONDITIONS." *International Journal of Structural Stability & Dynamics*, 12(06), 1053-1307.
- Esmaeily, A. (2013). "Special Issue on Experimental Methods in Damage Detection and Wind Engineering." *Journal of Engineering Mechanics Asce*, 139(3), 247-247.
- Results, S., Results, R. B. I., Remarks, C., Brent, M. P., Ph. D, Rolander, D. D., Graybeal, B. A., and Glenn, A. W., Ph. D (2001). "Reliability of Visual Bridge Inspection." *Public Roads*, 64.
- Nuruzzaman, M. "Digital Image Fundamentals in MATLAB."
- VikramPakrashi, FranckSchoefs, JeanBernardMemet, and AlanO'Connor (2010). "ROC dependent event isolation method for image processing based assessment of corroded harbour structures." *Structure & Infrastructure Engineering*, 6(3), 365-378.
- Abdelqader, I., Abudayyeh, O., and Kelly, M. E. (2003). "Analysis of Edge-Detection Techniques for Crack Identification in Bridges." *Journal of Computing in Civil Engineering*, 17(4), 255-263.
- Hutchinson, T. C., and Chen, Z. Q. (2006). "Improved Image Analysis for Evaluating Concrete Damage." *Journal of Computing in Civil Engineering*, 20(3), 210-216.
- Yamaguchi, T., and Hashimoto, S. (2010). "Fast crack detection method for large-size concrete surface images using percolation-based image processing." *Machine Vision & Applications*, 21(5), 797-809.
- Liu, Y. F., Cho, S., Spencer, B. F., and Fan, J. S. (2016). "Concrete Crack Assessment Using Digital Image Processing and 3D Scene Reconstruction." *Journal of Computing in Civil Engineering*, 30(1), 04014124.
- Ghorbani, R., Matta, F., and Sutton, M. A. (2014). *Full-Field Displacement Measurement and Crack Mapping on Masonry Walls Using Digital Image Correlation*, Springer International Publishing.
- Subirats, P., Dumoulin, J., Legeay, V., and Barba, D. "Automation of Pavement Surface Crack Detection using the Continuous Wavelet Transform." *Proc., IEEE International Conference on Image Processing*, 3037-3040.
- Zou, Q., Cao, Y., Li, Q., Mao, Q., and Wang, S. (2012). "CrackTree: Automatic crack detection from pavement images." *Pattern Recognition Letters*, 33(3), 227-238.
- Li, L., Sun, L., Tan, S., and Ning, G. (2012). "An Efficient Way in Image Preprocessing for Pavement Crack Images." *American Society of Civil Engineers*.
- Choi, K. Y., and Kim, S. S. (2005). "Morphological analysis and classification of types of surface corrosion damage by digital image processing." *Corrosion Science*, 47(1), 1-15.
- Lee, S., Chang, L. M., and Skibniewski, M. (2006). "Automated recognition of surface

- defects using digital color image processing." *Automation in Construction*, 15(4), 540-549.
- Ho, H. N., Kim, K. D., Park, Y. S., and Lee, J. J. (2013). "An efficient image-based damage detection for cable surface in cable-stayed bridges." *Ndt & E International*, 58(3), 18-23.
- Fukuda, Y., Feng, M. Q., Narita, Y., Kaneko, S. I., and Tanaka, T. (2013). "Vision-Based Displacement Sensor for Monitoring Dynamic Response Using Robust Object Search Algorithm." *IEEE Sensors Journal*, 13(12), 4725-4732.
- Cha, Y. J., You, K., and Choi, W. (2016). "Vision-based detection of loosened bolts using the Hough transform and support vector machines." *Automation in Construction*, 71, 181-188.
- Vu, H. V., Tran, N. H., Nguyen, T. V., and Hariharan, S. I. "Estimating information rates of Bernoulli-Gaussian impulsive noise channels in Rayleigh fading." *Proc., IEEE International Conference on Communications*, 1281-1285.
- Steger, C., Ulrich, M., and Wiedemann, C. (2007). *Machine Vision Algorithms and Applications*.
- Gupta, M. K. (2007). "Some novel digital image filters for suppression of impulsive noise."
- Canny, J. (1986). *A Computational Approach to Edge Detection*, IEEE Computer Society.
- Ramer, U. (1972). "An iterative procedure for the polygonal approximation of plane curves." *Computer Graphics & Image Processing*, 1(3), 244-256.
- Olver, P. J., and Tannenbaum, A. (2003). *Mathematical methods in computer vision*, Springer.